

Cite this: *Nanoscale*, 2012, **4**, 4183

www.rsc.org/nanoscale

PAPER

Electronic conductivity of alkyne-capped ruthenium nanoparticles†

Xiongwu Kang and Shaowei Chen*

Received 27th January 2012, Accepted 23rd February 2012

DOI: 10.1039/c2nr30213f

Ruthenium nanoparticles (2.12 ± 0.72 nm in diameter) were stabilized by the self-assembly of alkyne molecules (from 1-hexyne to 1-hexadecyne) onto the Ru surface by virtue of the formation of Ru–vinylidene interfacial linkages. Infrared measurements depicted three vibrational bands at 2050 cm^{-1} , 1980 cm^{-1} and 1950 cm^{-1} , which were ascribed to the vibrational stretches of the terminal triple bonds that were bound onto the nanoparticle surface. Thermogravimetric analysis showed that there were about 65 to 96 alkyne ligands per nanoparticle (depending on the ligand chainlength), corresponding to a molecular footprint of 20 to 15 \AA^2 . This suggests that the ligands likely adopted a head-on configuration on the nanoparticle surface, consistent with a vinylidene bonding linkage due to interfacial tautomeric rearrangements. With this conjugated interfacial bonding interaction, electronic conductivity measurements of the corresponding nanoparticle solid films showed that the nanoparticles all exhibited linear current–potential curves within the potential range of -0.8 V to $+0.8\text{ V}$ at varied temperatures (200 to 300 K). The ohmic characters were partly ascribed to the spilling of core electrons into the organic capping layer that facilitated interparticle charge transfer. Furthermore, based on the temperature dependence of the nanoparticle electronic conductivity, the activation energy for interparticle charge transfer was estimated to be in the range of 70 to 90 meV and significantly, the coupling coefficient (β) was found to be 0.31 \AA^{-1} for nanoparticles stabilized by short-chain alkynes (1-hexyne, 1-octyne, and 1-decyne), and 1.44 \AA^{-1} for those with long alkynes such as 1-dodecyne, 1-tetradecyne, and 1-hexadecyne. This may be accounted for by the relative contributions of the conjugated metal–ligand interfacial bonding interactions *versus* the saturated aliphatic backbones of the alkyne ligands to the control of interparticle charge transfer.

Introduction

A number of studies have demonstrated that the material properties of organically capped transition-metal nanoparticles can be tuned not only by the chemical nature of the metal cores and organic protecting ligands but also by the metal–ligand interfacial bonding interactions.¹ For example, when functional moieties are bound onto nanoparticle surfaces by conjugated metal–ligand linkages, effective intraparticle charge delocalization occurs, leading to the extended conjugation between the particle-bound functional groups and hence the emergence of novel optical and electronic properties that deviate markedly from those of the monomeric forms. This has been manifested by the intervalence charge transfer of ruthenium nanoparticles functionalized by ferrocenyl moieties with Ru=carbene π bonds or Ru–C \equiv $d\pi$ linkages.^{2–4} The behaviors are analogous to those

observed in organometallic complexes with multiple metal centers bridged by conjugated linkers.^{5–10} Intraparticle charge delocalization has also been observed with fluorophores such as pyrene and anthracene that are attached onto the nanoparticle surface by similar Ru=carbene π bonds, whereby the particle-bound fluorophores exhibit emission characteristics that are consistent with those of their dimeric derivatives.^{11–13} In other studies, using aryl diazonium salts as the precursors, transition-metal nanoparticles have been prepared by the grafting of the aryl radicals onto the metal surface forming metal–carbon covalent bonds, upon the addition of potent reducing reagents. Largely because of the diminishment of the metal–ligand interfacial resistance, the resulting nanoparticles exhibit an apparent enhancement of the electronic conductivity, as compared with that of the counterparts passivated by mercapto derivatives.^{14,15} As metal–organic linkages are a critical component in molecular electronics, it is of fundamental importance to examine the impacts of these interfacial bonding interactions on the ensemble charge transport dynamics, in particular, in light of the emergence of more diverse metal–ligand bonding interactions. This is the primary motivation of the present study.

Recently we demonstrated that ruthenium nanoparticles could also be passivated by the facile self-assembly of terminal

Department of Chemistry and Biochemistry, University of California, 1156 High Street, Santa Cruz, California 95064, USA. E-mail: shaowei@ucsc.edu

† Electronic supplementary information (ESI) available: TEM micrograph, derivative thermogravimetric curves, and UV-vis and fluorescence spectra of the alkyne-capped ruthenium nanoparticles. See DOI: 10.1039/c2nr30213f

alkynes,¹⁶ where the metal–ligand interfacial interactions involved a dynamic equilibrium between a side-on η^2 configuration and a head-on ruthenium–vinylidene linkage by virtue of a tautomeric rearrangement. The unique metal–ligand interfacial bonding interactions were manifested by the specific reactivity towards imine derivatives as well as olefin metathesis reactions with vinyl-terminated functional derivatives. In sharp contrast, no such activity was observed with ruthenium nanoparticles stabilized by the formation of Ru–C \equiv $d\pi$ linkages using alkynides (*i.e.*, deprotonated alkynes) as the precursors.⁴ Nevertheless, both nanoparticles exhibited similar photoluminescence properties, largely because of the conjugated nature of the metal–ligand interfacial interactions such that the particle-bound triple bonds behaved analogously to diacetylene derivatives.

In the present study, we investigate the interparticle charge transfer chemistry of the alkyne-capped ruthenium nanoparticles by measuring the electronic conductivity of the nanoparticle solid films at controlled temperatures. Experimentally, ruthenium nanoparticles were prepared by the self-assembly of alkyne molecules of different chainlengths (C_{*n*}H_{2*n*-2}, *n* = 6, 8, 10, 12, 14, and 16). The structures of the resulting nanoparticles were characterized by employing a variety of spectroscopic tools, and the electronic conductivity was assessed quantitatively by depositing particle films onto an interdigitated array (IDA) electrode. The energetic barrier for interparticle charge transfer as well as the coupling coefficient (β) were then evaluated. Remarkably, for nanoparticles capped with short alkynes (*n* = 6, 8, and 10), a very small value of β was found at 0.31 Å⁻¹, whereas for long capping alkynes (*n* = 12, 14, and 16), β was markedly greater at 1.44 Å⁻¹. The former is actually consistent with that observed with electron transfer through conjugated barriers, indicating the significant contributions of the conjugated metal–ligand interactions to the ensemble conductivity where extended spilling of core electrons facilitates interparticle charge transfer, whereas the latter is in good agreement with charge transfer through a saturated aliphatic spacer, likely a result of the dominant contribution from the long saturated molecular backbone of the ligands.

Experimental section

Chemicals

Ruthenium chloride (RuCl₃, 99+%, ACROS), 1-hexyne (Alfa Aesar, 98%), 1-octyne (Alfa Aesar, 98%), 1-decyne (TCI America), 1-dodecyne (ACROS, 98%), 1-tetradecyne (Wako), 1-hexadecyne (Alfa Aesar, 90%), 1,2-propanediol (ACROS), and sodium acetate trihydrate (NaOAc·3H₂O, MC&B) were used as received. All solvents were obtained from typical commercial sources and used without further treatment. Water was supplied by a Barnstead Nanopure water system (18.3 M Ω cm).

Preparation of ruthenium nanoparticles

The synthesis of 1-alkyne-stabilized Ru nanoparticles has been described in detail previously,¹⁶ which involved two key steps: (i) “bare” ruthenium colloids were prepared by thermolytic reduction of ruthenium chloride in 1,2-propanediol according to the procedure reported previously¹⁷ and (ii) a calculated amount of 1-alkynes was then added to the solution and the alkyne ligands

were self-assembled onto the Ru surface by the formation of Ru–vinylidene interfacial bonding linkages. In a typical reaction, 0.28 mmol of RuCl₃ and 2 mmol of NaOAc were dissolved in 200 mL of 1,2-propanediol. The mixed solution was heated to 165 °C for 1 h under vigorous stirring, where the solution turned dark brown signifying the formation of nanometre-sized ruthenium colloids. Transmission electron microscopic (TEM) measurements showed that the nanoparticles exhibited an average core diameter of 2.12 \pm 0.72 nm (Fig. S1 in the ESI†).¹⁷ Upon cooling to room temperature, the solution was split equally into six round-bottom flasks into which was added 1-alkynes (from 1-hexyne to 1-hexadecyne) dissolved in toluene at three-fold molar excess as compared to RuCl₃ under magnetic stirring overnight. An intense color appearance was observed in the toluene phase whereas the diol phase became colorless, indicating the extraction of the particles from the diol phase to the toluene phase as a result of the self-assembly of alkynes onto the nanoparticle surface. The toluene phase was then collected and dried by rotary evaporation, and the solids were rinsed extensively with ethanol to remove excessive free ligands. The resulting purified ruthenium nanoparticles were denoted as RuHC_{*n*} with *n* being the number of carbon atoms in the corresponding monomeric alkyne ligands.

Carbene-stabilized ruthenium nanoparticles were prepared by following a similar procedure, as described previously.¹⁷ Briefly, after the “bare” Ru colloids were prepared thermolytically, a toluene solution with a calculated amount of octyldiazoacetate (ODA) was added to the colloid solution, where carbene fragments were self-assembled onto the Ru nanoparticle surface forming Ru=carbene π bonds (and concurrently releasing nitrogen). The purified nanoparticles were referred to as Ru=C8.

Spectroscopy

¹H NMR spectroscopic measurements were carried out by using concentrated solutions of the nanoparticles in CDCl₃ with a Varian Unity 500 MHz NMR spectrometer. The absence of any sharp features indicated that the nanoparticles were free of excessive monomeric ligands. Thermogravimetric analysis (TGA) was carried out by using a Perkin-Elmer Pyris 1 instrument at a heating rate of 10 °C min⁻¹. UV-vis spectroscopic studies were performed with an ATI Unicam UV4 spectrometer using a 1 cm quartz cuvette with a resolution of 2 nm. Photoluminescence characteristics were examined with a PTI fluorospectrometer. FTIR measurements were carried out with a Perkin-Elmer FTIR spectrometer (Spectrum One, spectral resolution 4 cm⁻¹), where the samples were prepared by casting the particle solutions onto a KBr disk. X-Ray photoelectron spectra (XPS) were recorded with a PHI 5400/XPS instrument equipped with an Al K α source operated at 350 W and at 10⁻⁹ Torr. Silicon wafers were sputtered by argon ions to remove carbon from the background and used as substrates. The spectra were charge-referenced to the Au 4f_{7/2} peak (83.8 eV) of sputtered gold.

Electronic conductivity

For electronic conductivity measurements, a particle film was formed by dropcasting 1 μ L of a concentrated particle solution in toluene (60 mg mL⁻¹) onto an interdigitated array (IDA)

electrode (25 pairs of gold fingers of $3 \text{ mm} \times 5 \mu\text{m} \times 5 \mu\text{m}$, from ABTECH). At least 30 min was allowed for solvent evaporation, and the film thickness was found to be greater than the height of the IDA fingers. Conductivity measurements were then carried out in vacuum (Cryogenic Equipment, JANIS CO) with a CHI710 Electrochemical Workstation at different temperatures (Lakeshore 331 Temperature Controller). The ensemble conductivity (σ) was evaluated by the equation $\sigma = \left(\frac{1}{49R}\right)\left(\frac{L}{S}\right)$, where R is the ensemble resistance calculated from the slope of the I - V curves, L is the IDA electrode interfinger gap ($5 \mu\text{m}$), and S is the film cross-sectional area approximated by (finger height, $5 \mu\text{m}$) \times (finger length, 3 mm). The constant (49) indicates that there are totally 49 junctions which are in parallel within the IDA chip.

Results and discussion

The structures of the alkyne capping ligands were first examined by FTIR measurements, as depicted in Fig. 1. The most significant observation is the disappearance of the $\equiv\text{C-H}$ vibrational stretch at 3314 cm^{-1} , the $\equiv\text{C-H}$ bend overtone at 1255 cm^{-1} and the $\equiv\text{C-H}$ bend fundamental at 631 cm^{-1} , all of which are well-defined with monomeric alkynes.¹⁸ At first glance, this is somewhat surprising. In our previous study with ruthenium nanoparticles capped by acetylide derivatives,⁴ we observed the disappearance of these vibrational features, because of the deprotonation of the alkyne ligands. Yet, in the present study, alkyne molecules were used instead. The fact that these unique infrared characteristics were no longer present may be ascribed to the dynamic equilibrium between the η^2 configuration and vinylidene linkage at the metal–ligand interface.¹⁶ In fact, such an observation was also reported in earlier studies of the binding of alkynes onto Au and Ag surfaces by surface-enhanced Raman spectroscopy (SERS).¹⁹ Furthermore, the lack of the $\equiv\text{C-H}$ vibrational stretches also confirms that the ruthenium nanoparticles were spectroscopically clean without excessive free ligands.

Another interesting feature is the appearance of multiple peaks in the triple bond region (1900 – 2100 cm^{-1}), where all

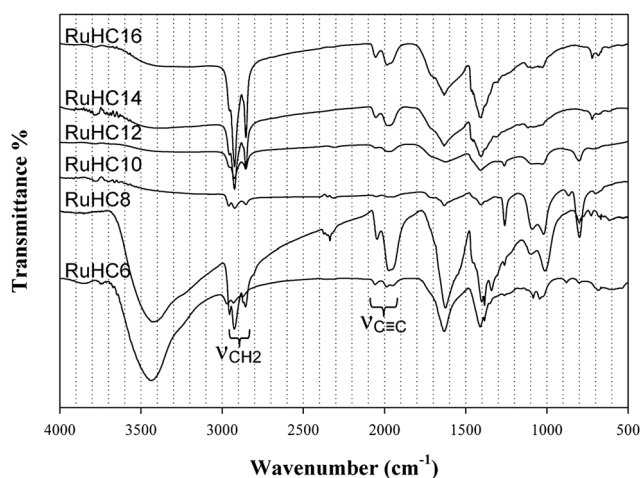


Fig. 1 FTIR spectra of ruthenium nanoparticles capped with varied 1-alkynes.

nanoparticle samples exhibited a pair of strong peaks at *ca.* 1950 cm^{-1} and 1976 cm^{-1} and a relatively weaker one at 2056 cm^{-1} . Similar observations were reported with alkynes bound onto Au and Ag surfaces by SERS measurements.¹⁹ Note that for monomeric alkynes, the $\text{C}\equiv\text{C}$ vibrational stretch is typically well-defined with a single peak at 2119 cm^{-1} .¹⁸ This marked discrepancy strongly suggests that the alkyne molecules were indeed chemically bonded onto the Ru surface, and the decreasing bonding order (lower peak wavenumbers) might be attributed to the σ - π bonding interactions between the triple-bond moieties and the ruthenium metal cores.

In addition, the packing of the nanoparticles within the solid films may be evaluated by the methylene (CH_2) vibrational stretches. This is to take advantage of the sensitive variation of these vibrational features to the ordering of the alkyl chains.^{20,21} For instance, in crystalline polyethylene, the antisymmetric (d^-) and symmetric (d^+) CH_2 vibrational stretches are observed at 2920 cm^{-1} and 2850 cm^{-1} , respectively, whereas in solution, they increase to 2928 cm^{-1} and 2856 cm^{-1} . In the present study, one can see from Fig. 1 that for ruthenium nanoparticles capped with long alkyne molecules ($n = 10$ to 16), the d^- and d^+ bands appear at 2923 cm^{-1} and 2853 cm^{-1} , respectively, whereas for RuHC8 nanoparticles, they increase slightly to 2925 cm^{-1} and 2856 cm^{-1} , and for RuHC6 nanoparticles, to even higher values of 2930 cm^{-1} and 2874 cm^{-1} . This observation suggests that in the nanoparticle solid ensembles, the packing order of the nanoparticle-bound alkyne ligands increased with increasing chainlength of the molecules, consistent with earlier observations, for instance, with alkanethiolate-protected gold nanoparticles.²²

The coverage of the alkyne ligands on the nanoparticle surface was then quantified by TGA measurements. Fig. 2 shows the weight loss curves of the six ruthenium nanoparticles. It can be seen that for all particle samples, the weight loss commences at about $150 \text{ }^\circ\text{C}$, exhibits an abrupt transition and ends at higher temperatures. Table 1 lists the transition temperature (T_g , defined by the first-order derivative of the weight loss curves, Fig. S2†) and organic weight contents for the nanoparticles. It can be seen that both the transition temperature and total weight

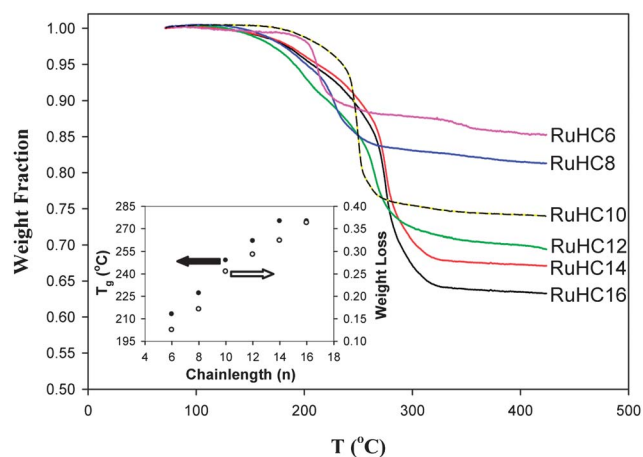


Fig. 2 TGA curves of ruthenium nanoparticles capped with varied 1-alkynes. Inset shows the variations of the transition temperature (T_g , ●) and weight loss (○) of these nanoparticles with the chainlength (n) of the alkyne ligands ($\text{C}_n\text{H}_{2n-2}$).

Table 1 Summary of structural properties of ruthenium nanoparticles capped by varied alkynes: weight loss transition temperatures (T_g), organic weight contents, numbers of alkyne ligands on the nanoparticle surface, and activation energy (E_a) of interparticle charge transfer

Sample	RuHC6	RuHC8	RuHC10	RuHC12	RuHC14	RuHC16
$T_g/^\circ\text{C}$	213	227	249	262	275	275
Organic weight (%)	12.5	17.1	25.5	29.3	32.4	36.3
Number of ligands	65.1	70.1	92.7	93.3	92.4	96.0
Ligand footprint/ \AA^2	21.7	20.1	15.2	15.1	15.3	14.7
E_a/meV	69.0	66.6	63.6	67.1	72.3	87.2

loss display a linear increment with the chainlength of the alkyne capping ligands, as shown respectively by the filled and open circles in the inset of Fig. 2. For instance, when the chainlength of the nanoparticle capping ligands increases from $n = 6$ (1-hexyne) to $n = 16$ (1-hexadecyne), T_g increases from 213 °C to 275 °C. This may be ascribed to the enhanced van der Waals interactions between the organic capping ligands that improve the thermal stability of the nanoparticles. Meanwhile, the organic content increases from 12.5% to 36.3%, which was exploited for the quantitative evaluation of the number of alkyne ligands on the nanoparticle surface: RuHC6, 65.1; RuHC8, 70.1; RuHC10, 92.7; RuHC12, 93.3; RuHC14, 92.4; and RuHC16, 96.0, corresponding to an average footprint of the capping ligands of *ca.* 20 \AA^2 for RuHC6 and RuHC8 and 15 \AA^2 for nanoparticles with longer alkyne ligands ($n = 10$ to 16), as listed in Table 1. Such a discrepancy is in agreement with the ligand packing order as manifested in the FTIR measurements presented above (Fig. 1). Note that in the previous study where the ruthenium nanoparticles were capped with 1-octynide ligands,⁴ the average footprint of the capping ligands was about 15 \AA^2 . These results suggest that the alkyne ligands most probably adopted a “vertical” head-on configuration on the ruthenium surface, consistent with the conjugated metal–ligand interfacial interactions involving ruthenium–vinylidene bonds, as proposed earlier.¹⁶

The interfacial bonding interactions were further examined by XPS measurements. Fig. 3 shows the representative XPS survey spectra (black curves) of the RuHC12 (bottom spectrum) and Ru=C8 (top spectrum) nanoparticles, within the binding energy range of 278 and 289 eV. There are two well-defined peaks with both nanoparticles. The peak at 280.45 may be ascribed to Ru3d_{5/2}, slightly higher than that of metallic ruthenium (which typically exhibits two peaks at 280.2 eV and 284.3 eV for the 3d_{5/2} and 3d_{3/2} electrons, respectively),^{23,24} suggesting possible electron transfer from Ru to the alkyne ligands. For the peak at 284.57 eV, it is most likely due to the combined contributions from both Ru3d_{3/2} and C1s electrons. Note that carbon 1s electrons in sp³, sp² and sp hybridization in general display a binding energy of 285.0 eV,²⁵ 284.4 eV, and 283.5 eV,^{26–30} respectively. In fact, deconvolution of the bottom spectrum yields a peak at 284.36 eV for Ru3d_{3/2} (magenta curve), 284.94 eV for sp³ C1s (blue curve), 283.79 eV for sp² C1s (light blue curve), and 283.37 eV for sp C1s (grey curve). These assignments were further confirmed by a comparison with the Ru=C8 nanoparticles (top spectrum),

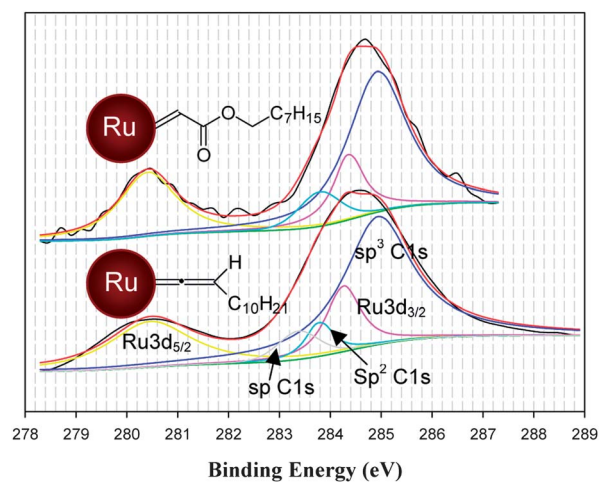


Fig. 3 XPS survey spectra of the (bottom) RuHC12 and (top) Ru=C8 nanoparticles which are deconvoluted to resolve individual components. Black curves are the experimental data and red curves are the summation of the fitting peaks (blue, magenta, yellow, light blue, and grey curves) plus backgrounds (green curves).

where the Ru3d_{3/2} and C1s (sp³ and sp²) electrons can be clearly identified and no sp C1s can be resolved, as anticipated with the formation of Ru=carbene π bonding linkage at the metal–ligand interface.¹⁷ Note that in both nanoparticle samples, the curve fittings were carried out by fixing the area ratios based on the nanoparticle structure as depicted in the figure, and it can be seen that the fittings (peak sum, red curves) were in excellent agreement with the experimental data (black curves). Significantly, the fact that sp, sp² and sp³ electrons can all be seen with the alkyne-capped Ru nanoparticles is again consistent with the structural model where tautomeric rearrangements occurred at the metal–ligand interface leading to the dynamic formation of a ruthenium–vinylidene (Ru=C=CHC₁₀H₂₁) interfacial linkage.¹⁶

With the conjugated interfacial linkage, the alkyne-capped nanoparticles exhibited apparent photoluminescence, although UV-vis measurements only showed a featureless exponential decay profile that is characteristic of nanosized metal particles (due to the so-called Mie scattering),³¹ as manifested in Fig. S3†. From the excitation and emission spectra of the ruthenium nanoparticles capped by varied 1-alkynes, it can be seen that similar to the results reported in our previous study,¹⁶ all nanoparticles exhibited a well-defined excitation peak at 360 nm and an emission peak at 440 nm, regardless of the chainlength of the alkyne ligands. This is ascribed to the conjugated metal–ligand interfacial interactions that rendered the particle-bound triple bonds to behave analogously to diacetylene moieties. In fact, the photoluminescence characteristics observed here are consistent with those of diacetylene derivatives.⁴

The impacts of the conjugated metal–ligand interfacial interactions on the electronic conductivity of the nanoparticles were then examined by electrochemical measurements with nanoparticle dropcast films. Fig. 4 shows the current–potential (I – V) profiles at controlled temperatures of solid films of the alkyne-capped ruthenium nanoparticles which were prepared by dropcasting 1 μL of a 60 mg mL^{−1} particle solution in toluene

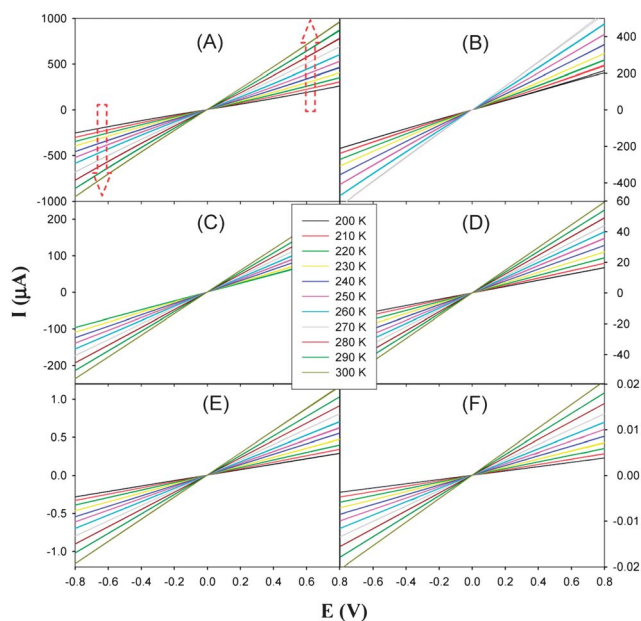


Fig. 4 Current–potential (I – V) curves of solid films of ruthenium nanoparticles capped by varied 1-alkynes at different temperatures (shown as figure legends): (A) RuHC6, (B) RuHC8, (C) RuHC10, (D) RuHC12, (E) RuHC14, and (F) RuHC16. Potential scan rate 10 mV s^{-1} .

onto an IDA surface. It can be seen that within the bias voltage range of -0.8 V to $+0.8 \text{ V}$, the I – V curves of all nanoparticle samples exhibited clearly linear profiles, suggesting rather efficient interparticle charge transfer. Note that the ohmic characters have been observed extensively in the assessments of the electronic conductivity of nanoparticle solids, where interparticle charge transfer was interpreted on the basis of a thermally activated hopping mechanism.^{14,15} In addition, the ensemble currents increased with increasing temperature from 200 to 300 K. Such semiconducting characteristics are consistent with the composite nature of the nanoparticle materials.

It should be noted that in nanoparticle solids, the metallic cores are embedded within an organic matrix resulting from the intercalation of the surface protecting ligands between neighboring particles, and interparticle charge transfer occurs by a percolation process that is determined by electron tunneling between adjacent metal cores through the organic layers. Thus, the resulting currents strongly depend on the physical barrier of the tunneling junction, which is defined by the edge-to-edge distance between the nanoparticles and is in general assumed to be equal to one fully extended chainlength of the capping ligands (because of ligand intercalation). That is, the nanoparticle ensemble conductivity (σ) may be expressed by the following equation,^{32,33}

$$\sigma = \sigma_0 e^{-\beta\delta} e^{-\frac{E_a}{RT}} \quad (1)$$

where σ_0 represents the intrinsic electronic conductivity of the nanoparticle films, β the electronic coupling coefficient, δ the edge-to-edge interparticle separation, E_a the activation energy for interparticle charge transfer, R the gas constant, and T the temperature.

Fig. 5(A) depicts the variation of the electronic conductivity (σ) of the varied nanoparticles within the temperature range of 200 to 300 K. First, it can be seen that indeed all nanoparticle

samples exhibited a well-defined exponential decrease of the ensemble conductivity with increasing reciprocal temperature ($1/T$), consistent with thermally activated interparticle charge transfer (eqn (1)). From the linear regressions, the activation energy (E_a) for interparticle charge transfer was then estimated (Table 1): 69.0 meV, RuHC6; 66.6 meV, RuHC8; 63.6 meV, RuHC10; 67.1 meV, RuHC12; 72.3 meV, RuHC14; and 87.2 meV, RuHC16. One can see that these energetic barriers are actually quite close to each other, but markedly lower than those observed with solid films of alkanethiolate-passivated gold nanoparticles prepared in a similar fashion,³⁴ which may be accounted for by the conjugated metal–ligand interfacial linkage that lowers the interfacial contact resistance and hence facilitates interparticle charge transfer, in comparison with the metal–sulfur bonds.

Second, one can see that with increasing chainlength (δ) of the capping alkyne ligands, the ensemble conductivity decreases accordingly. For instance, the electronic conductivity of the nanoparticles at 270 K can be found at 5.71 mS m^{-1} , RuHC6; 3.46 mS m^{-1} , RuHC8; 1.47 mS m^{-1} , RuHC10; 0.37 mS m^{-1} ,

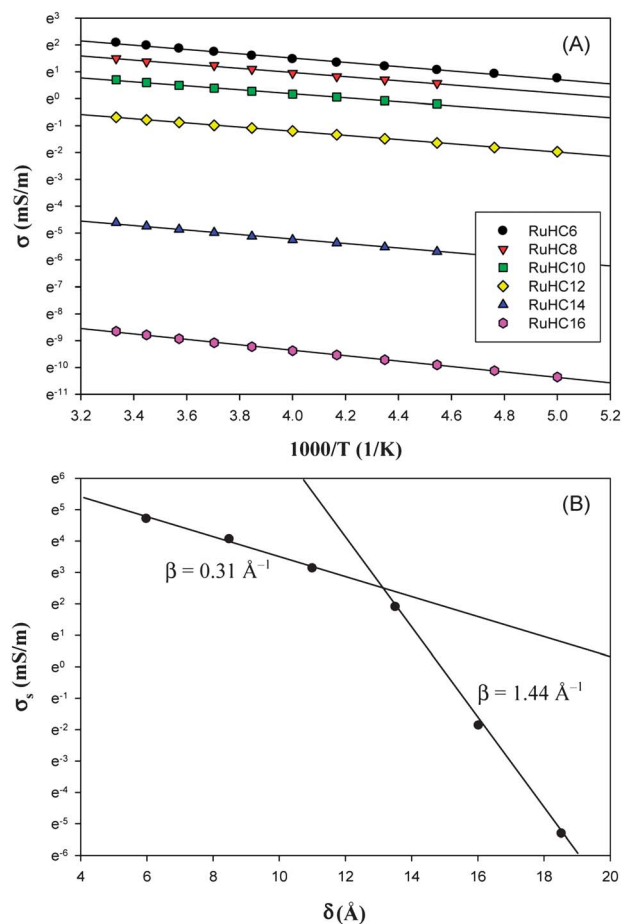


Fig. 5 (A) Variation of the electronic conductivity of the alkyne-capped ruthenium nanoparticles with temperature. Symbols are experimental data acquired from Fig. 4 and lines are the corresponding linear regressions. (B) Variation of the nanoparticle electronic conductivity (σ_s) at infinite temperature with the chainlength of the alkyne ligands. Symbols are experimental data estimated from the intercepts in panel (A) and lines are the corresponding linear regressions.

RuHC12; $6.82 \times 10^{-3} \text{ mS m}^{-1}$, RuHC14; and $1.14 \times 10^{-4} \text{ mS m}^{-1}$, RuHC16. These are about 10 to 14 orders of magnitude lower than that of metallic ruthenium ($1.41 \times 10^7 \text{ S m}^{-1}$ at 273 K),³⁵ which may again be ascribed to the composite nature of the nanoparticles.

Further comparison can be made by the variation of the nanoparticle conductivity at infinite temperature ($\sigma_s = \sigma_o e^{-\beta\delta}$, acquired from the intercepts of the linear regressions in panel (A)) with ligand chainlength (δ , estimated by Hyperchem®), as shown in panel (B). From eqn (1), one would anticipate an exponential decay of the nanoparticle electronic conductivity with ligand chainlength (δ).³² Yet from the semilog plot in Fig. 5(B), it can be seen that the experimental profile actually consists of two linear segments, with two distinctly different slopes, which define the electronic coupling coefficients (β). For the ruthenium nanoparticles capped by short alkyne ligands ($n = 6, 8, \text{ and } 10$), β can be estimated to be *ca.* 0.31 \AA^{-1} , whereas for those with long alkynes ($n = 12, 14, \text{ and } 16$), $\beta = 1.44 \text{ \AA}^{-1}$. It should be noted that β is highly dependent on the chemical nature of the electron tunneling pathway. For conjugated spacers, the β values are typically in the range of 0.4 to 0.6 \AA^{-1} , whereas with saturated linkers, β increases to around 1.0 \AA^{-1} .^{36–39} In other words, the low β observed with the nanoparticles capped by short alkynes suggests that the ligand layers actually behave analogously to conjugated linkers for interparticle charge transfer. This may be ascribed to the conjugated metal–ligand interfacial bonding interactions that allows for effective spilling of core electrons into the organic protecting layers and thus enhances electronic coupling between neighboring particles. In contrast, for nanoparticles capped with long alkyne ligands, this interfacial contribution becomes insignificant and the primary barrier to interparticle charge transfer arises from the saturated fragments of the molecule backbones, as reflected by the high β value observed above.

It should be noted that the above analysis was based on the assumption that the nanoparticle capping ligands were fully intercalated and hence δ was equal to the chainlength of a single molecule. Yet, deviations might appear, especially for long alkynes where the high packing order, as manifested above in FTIR and TGA measurements, was likely to impede the full intercalation of surface ligands between neighboring particles. That is, the large β values observed for $n = 12, 14, \text{ and } 16$, as compared with that observed previously with saturated spacers ($\sim 1.0 \text{ \AA}^{-1}$),^{36–39} might be somewhat overestimated, partly due to an underestimation of the δ values. On the other hand, for all the nanoparticles to have the same β value of 0.31 \AA^{-1} , δ would have to be 1.1, 1.7, and 2.0 times that of a single ligand chainlength for $n = 12, 14, \text{ and } 16$, respectively. This implies little or even zero intercalation of the surface ligands for the RuHC14 and RuHC16 nanoparticles. Thus, the actual interparticle separation most likely fell in the intermediate range between $1\times$ and $2\times$ the molecular chainlength. Further studies by, for instance, small-angle X-ray diffraction,⁴⁰ are desired to unravel these structural details.

Conclusion

Ruthenium nanoparticles were stabilized by the self-assembly of 1-alkyne molecules of different chainlength forming

a ruthenium–vinylidene interfacial linkage through an interfacial tautomeric rearrangement. Multiple vibrational bands appeared in the triple-bond region in FTIR measurements, whereas no vibrational features of the terminal $\equiv\text{C–H}$ were observed. These results suggested that indeed the ligands were bound onto the nanoparticle surface. TGA measurements were carried out to quantify the number of alkyne ligands on the nanoparticle surface, from which the average molecular footprint was estimated to be 15 to 20 \AA^2 , consistent with a head-on configuration of the alkyne ligands on the Ru surface. The formation of a conjugated metal–ligand interfacial bond was further evidenced in XPS and photoluminescence measurements, which was found to facilitate interparticle charge transfer. Based on the temperature dependence of the nanoparticle electronic conductivity, the energetic barrier was estimated to be *ca.* 70 to 90 meV, substantially lower than that observed with solid films of alkanethiolate-passivated gold nanoparticles. More interestingly, the electronic coupling coefficient β was found to be 0.31 \AA^{-1} for nanoparticles capped with short alkynes such as hexyne, octyne and decyne, whereas a much higher value (1.44 \AA^{-1}) was observed for those stabilized by long alkynes of dodecyne, tetradecyne and hexadecyne. This was attributed to the conjugated interfacial bonding linkage that allowed for more extensive spilling of core electrons into the organic protecting layer. For short capping ligands, these interfacial contributions were significant in enhancing interparticle electronic interactions and hence interparticle charge transfer; whereas for long alkyne ligands, the saturated aliphatic fragments within the molecular backbones became the dominant spacers in interparticle charge transfer. These results further highlight the fundamental importance of metal–organic contacts in the manipulation of interfacial charge transfer, a common and yet critical feature in nano/molecular electronics.

Acknowledgements

This work was supported, in part, by the National Science Foundation (CHE—1012256) and the ACS-Petroleum Research Fund (49137-ND10). XPS and TEM studies were carried out at the Molecular Foundry and National Center for Electron Microscopy, Lawrence Berkeley National Laboratory as part of a user project.

Notes and references

- 1 S. W. Chen, *Electroanalytical Chemistry*, ed. A. J. Bard and C. G. Zoski, 2010, vol. 23, p. 171.
- 2 W. Chen, S. W. Chen, F. Z. Ding, H. B. Wang, L. E. Brown and J. P. Konopelski, *J. Am. Chem. Soc.*, 2008, **130**, 12156.
- 3 W. Chen, L. E. Brown, J. P. Konopelski and S. W. Chen, *Chem. Phys. Lett.*, 2009, **471**, 283.
- 4 W. Chen, N. B. Zuckerman, X. W. Kang, D. Ghosh, J. P. Konopelski and S. W. Chen, *J. Phys. Chem. C*, 2010, **114**, 18146.
- 5 D. O. Cowan, C. Levanda, J. Park and F. Kaufman, *Acc. Chem. Res.*, 1973, **6**, 1.
- 6 P. Day, N. S. Hush and R. J. H. Clark, *Philos. Trans. R. Soc. London, Ser. A*, 2008, **366**, 5.
- 7 D. R. Gamelin, E. L. Bominaar, C. Mathoniere, M. L. Kirk, K. Wiegardt, J. J. Girerd and E. I. Solomon, *Inorg. Chem.*, 1996, **35**, 4323.
- 8 R. D. Williams, V. I. Petrov, H. P. Lu and J. T. Hupp, *J. Phys. Chem. A*, 1997, **101**, 8070.

- 9 B. S. Brunschwig, C. Creutz and N. Sutin, *Chem. Soc. Rev.*, 2002, **31**, 168.
- 10 H. Sun, J. Steeb and A. E. Kaifer, *J. Am. Chem. Soc.*, 2006, **128**, 2820.
- 11 W. Chen, N. B. Zuckerman, J. W. Lewis, J. P. Konopelski and S. W. Chen, *J. Phys. Chem. C*, 2009, **113**, 16988.
- 12 W. Chen, N. B. Zuckerman, J. P. Konopelski and S. W. Chen, *Anal. Chem.*, 2010, **82**, 461.
- 13 W. Chen, S. Pradhan and S. W. Chen, *Nanoscale*, 2011, **3**, 2294.
- 14 D. Ghosh and S. W. Chen, *J. Mater. Chem.*, 2008, **18**, 755.
- 15 D. Ghosh, S. Pradhan, W. Chen and S. W. Chen, *Chem. Mater.*, 2008, **20**, 1248.
- 16 X. W. Kang, N. B. Zuckerman, J. P. Konopelski and S. W. Chen, *J. Am. Chem. Soc.*, 2012, **134**, 1412.
- 17 W. Chen, J. R. Davies, D. Ghosh, M. C. Tong, J. P. Konopelski and S. W. Chen, *Chem. Mater.*, 2006, **18**, 5253.
- 18 R. M. Silverstein, G. C. Bassler and T. C. Morrill, *Spectrometric Identification of Organic Compounds*, Wiley, 1991.
- 19 H. Feilchenfeld and M. J. Weaver, *J. Phys. Chem.*, 1989, **93**, 4276.
- 20 R. G. Snyder, H. L. Strauss and C. A. Elliger, *J. Phys. Chem.*, 1982, **86**, 5145.
- 21 R. G. Snyder, M. Maroncelli, H. L. Strauss and V. M. Hallmark, *J. Phys. Chem.*, 1986, **90**, 5623.
- 22 M. J. Hostetler, J. J. Stokes and R. W. Murray, *Langmuir*, 1996, **12**, 3604.
- 23 N. Chakroune, G. Viau, S. Ammar, L. Poul, D. Veautier, M. M. Chehimi, C. Mangeney, F. Villain and F. Fievet, *Langmuir*, 2005, **21**, 6788.
- 24 R. Luque, J. H. Clark, K. Yoshida and P. L. Gai, *Chem. Commun.*, 2009, 5305.
- 25 S. Zhang, K. L. Chandra and C. B. Gorman, *J. Am. Chem. Soc.*, 2007, **129**, 4876.
- 26 M. Rybachuk and J. M. Bell, *Carbon*, 2009, **47**, 2481.
- 27 S. Turgeon and R. W. Paynter, *Thin Solid Films*, 2001, **394**, 44.
- 28 U. Dettlaff-Weglikowska, J. M. Benoit, P. W. Chiu, R. Graupner, S. Lebedkin and S. Roth, *Curr. Appl. Phys.*, 2002, **2**, 497.
- 29 G. Iucci, V. Carravetta, P. Altamura, M. V. Russo, G. Paolucci, A. Goldoni and G. Polzonetti, *Chem. Phys.*, 2004, **302**, 43.
- 30 K. Siegbahn, *Philos. Trans. R. Soc. London, Ser. A*, 1970, **268**, 33.
- 31 J. A. Creighton and D. G. Eadon, *J. Chem. Soc., Faraday Trans.*, 1991, **87**, 3881.
- 32 G. N. R. Wang, L. Y. Wang, R. D. Qiang, J. G. Wang, J. Luo and C. J. Zhong, *J. Mater. Chem.*, 2007, **17**, 457.
- 33 R. H. Terrill, T. A. Postlethwaite, C. H. Chen, C. D. Poon, A. Terzis, A. D. Chen, J. E. Hutchison, M. R. Clark, G. Wignall, J. D. Londono, R. Superfine, M. Falvo, C. S. Johnson, E. T. Samulski and R. W. Murray, *J. Am. Chem. Soc.*, 1995, **117**, 12537.
- 34 S. Pradhan, J. Sun, F. J. Deng and S. W. Chen, *Adv. Mater.*, 2006, **18**, 3279.
- 35 D. R. Lide, *CRC Handbook of Chemistry and Physics: A Ready-Reference Book of Chemical and Physical Data*, CRC Press, 2004.
- 36 S. Creager, C. J. Yu, C. Bamdad, S. O'Connor, T. MacLean, E. Lam, Y. Chong, G. T. Olsen, J. Y. Luo, M. Gozin and J. F. Kayyem, *J. Am. Chem. Soc.*, 1999, **121**, 1059.
- 37 R. E. Holmlin, R. Haag, M. L. Chabinye, R. F. Ismagilov, A. E. Cohen, A. Terfort, M. A. Rampi and G. M. Whitesides, *J. Am. Chem. Soc.*, 2001, **123**, 5075.
- 38 B. C. Sih, A. Teichert and M. O. Wolf, *Chem. Mater.*, 2004, **16**, 2712.
- 39 S. B. Sachs, S. P. Dudek, R. P. Hsung, L. R. Sita, J. F. Smalley, M. D. Newton, S. W. Feldberg and C. E. D. Chidsey, *J. Am. Chem. Soc.*, 1997, **119**, 10563.
- 40 H. Noh, A. M. Hung and J. N. Cha, *Small*, 2011, **7**, 3021.